


Emergent transverse-field Ising model in d^4 spin-orbit Mott insulators

 Jiří Chaloupka 

Department of Condensed Matter Physics, Faculty of Science, Masaryk University, Kotlářská 2, 61137 Brno, Czech Republic



(Received 30 August 2023; accepted 3 January 2024; published 16 January 2024)

Mott-insulating transition metal oxides containing t_{2g}^4 ions with strong spin-orbit coupling were recently demonstrated to display unusual magnetism due to a dynamical mixing of the low-energy multiplet states via exchange processes. Here we derive exchange interactions in the situation where a tetragonal or trigonal crystal field selects a single relevant excited state on top of the singlet ionic ground state, producing an effective spin- $\frac{1}{2}$. We show that these moments universally obey antiferromagnetic transverse-field Ising model (TFIM) with an intrinsic transverse field generated by the splitting of the two ionic singlets. Using Ru^{4+} as a example ion, we provide quantitative estimates of the exchange and illustrate the emergent TFIM physics based on phase diagrams and excitation spectra obtained for several 2D lattices—square, honeycomb, as well as for the frustrated triangular lattice.

 DOI: [10.1103/PhysRevB.109.L020403](https://doi.org/10.1103/PhysRevB.109.L020403)

Introduction. Transverse-field Ising model introduced by de Gennes in 1960s [1] ranks among the most prominent example systems to study quantum criticality [2,3]. Its Ising part belongs to a few lattice models in statistical physics for which exact solutions are available [4–9] and gained popularity as a prototype model to capture collective behavior not only of localized spins in magnets but also in a much broader context [10,11]. Ising model itself represents a classical problem. By adding transverse magnetic field, the quantum nature of spins comes into play, leading to a quantum critical behavior reflecting a competition of Ising interactions and Zeeman energy. The model has been studied in various settings, a particularly appealing case is the antiferromagnetic (AF) TFIM on a triangular lattice combining quantum criticality with frustration and exhibiting Berezinskii-Kosterlitz-Thouless (BKT) transitions [12–14].

Realization of TFIM in magnetic materials is limited by the requirement of strong uniaxial anisotropy of exchange interactions and their suitable strength with respect to accessible magnetic fields. Simple anisotropic ferromagnets were considered since the early days [15]; however, a definitive experimental demonstration came only in 2010 with CoNb_2O_6 acting as 1D TFIM chain in neutron scattering [16]. The case of frustrated AF TFIM is yet more delicate. A promising route was recently suggested by $4f$ triangular-lattice compound TmMgGaO_4 where signatures of BKT physics were observed [17–19]. Here the lowest two levels of Tm^{3+} ions form a well-isolated pair of singlets hosting effective spin- $\frac{1}{2}$. Thanks to large spin-orbit coupling (SOC) and hence large orbital component of these moments, they are subject to strongly anisotropic interactions. The second key ingredient is the crystal-field (CF) induced splitting of the two singlets that plays a role of an *intrinsic* transverse field [20–23]. In this Letter we show that $4d^4$ and $5d^4$ Mott insulators with large SOC [24] may be even more convenient platform for TFIM utilizing a similar mechanism. As we demonstrate by explicitly deriving the exchange model, at sufficiently large negative CF splitting of t_{2g} levels, the interactions are of AF Ising-type

enforced by the very structure of the d^4 ionic states. This promises a realization of TFIM on various 2D lattices at larger energy scales and corresponding characteristic temperatures as compared to $4f$ systems (exchange strength reaching tens of meV compared to ≈ 1 meV for TmMgGaO_4 [17]), with the intrinsic transverse field potentially tunable by straining.

TFIM imposed by spin-orbital structure of ionic states. We first briefly review the multiplet structure of relevant ions such as Ru^{4+} or Ir^{5+} with d^4 valence configuration limited to t_{2g} orbitals. Large SOC in these ions forms nonmagnetic $J = 0$ singlet ground state s and low-energy $J = 1$ triplet excitations T_x, T_y, T_z separated from the ground-state level by energy $\zeta/2$ with ζ denoting the single-electron SOC strength [24]. These states may serve as a basis for an effective model exhibiting quantum critical behavior due to the competition of exchange and triplet energy cost [24,25]. The essential control parameter here is the tetragonal or trigonal CF splitting Δ of t_{2g} orbital levels relevant for 2D lattices of corner-sharing or edge-sharing metal- O_6 octahedra, respectively. Nonzero Δ splits the $J = 1$ triplet and strongly modifies the ionic excitation energies as plotted in Fig. 1(a) and thoroughly discussed within the Supplemental Material (SM) [26]. Earlier studies analyzed the situation with no triplet splitting [25,27,28] and partially the positive- Δ case [29,30]. Here we focus on the so-far unexplored negative- Δ case with $|\Delta| \gtrsim \zeta$, the relevant set of basis states thus gets reduced to a non-Kramers doublet consisting of the ionic ground state s and one of the triplets T_z selected by the out-of-plane CF axis direction z [see Figs. 1(a) and 1(e)]. The internal structure of these t_{2g}^4 states sketched in Fig. 1(b) is best appreciated when expressing them via eigenstates $|L_z, S_z\rangle$ of the total effective t_{2g} orbital momentum $L = 1$ and total spin $S = 1$ carried by the two t_{2g} holes,

$$\begin{aligned}
 |s\rangle &= \frac{1}{\sqrt{2}}(|+1, -1\rangle + |-1, +1\rangle) \cos \vartheta_0 - |0, 0\rangle \sin \vartheta_0, \\
 |T_z\rangle &= \frac{i}{\sqrt{2}}(|+1, -1\rangle - |-1, +1\rangle).
 \end{aligned} \tag{1}$$

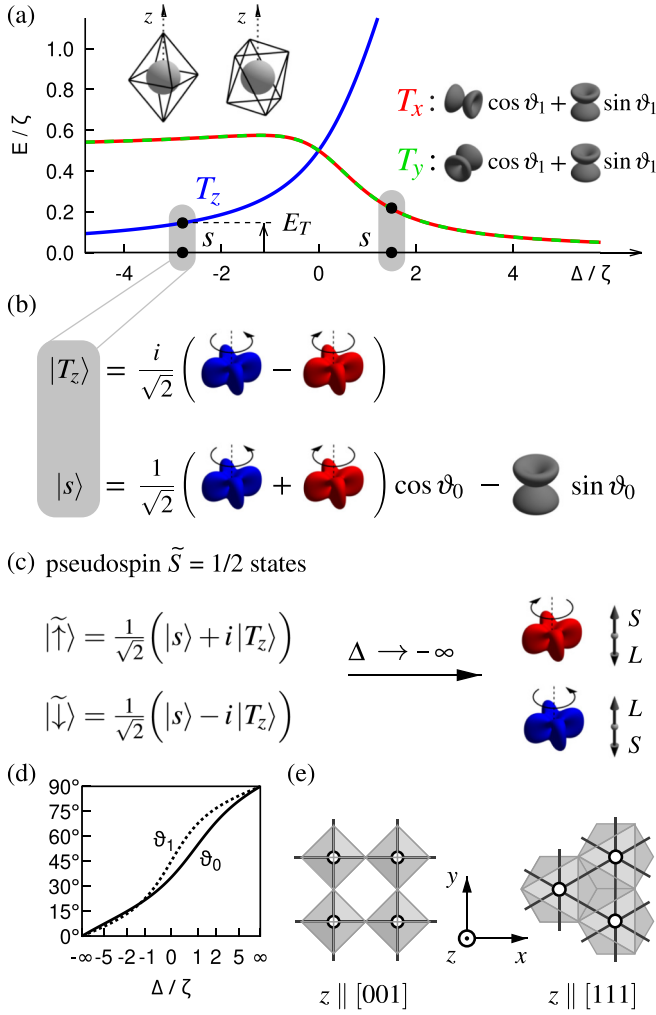


FIG. 1. (a) Low-energy levels of t_{2g}^4 ion depending on tetragonal or trigonal CF splitting Δ . The energies are plotted relative to the ionic ground-state level. Within LS coupling scheme, total $L = 1$ and $S = 1$ of the two holes added to the t_{2g}^6 configuration are combined by SOC into ground-state singlet s , a triplet of states $T_{x,y,z}$ degenerate at $\Delta = 0$, and a quintuplet at higher energies that may be ignored. In point-charge model, negative Δ corresponds to the indicated tetragonal/trigonal elongation of metal- O_6 octahedra (in reality it is influenced also by the Madelung potential contributed by more distant ions and covalency effects, which may break this simple correspondence). (b) At large enough $\Delta < 0$, the pair s and T_z forms the basis of the low-energy model. The corresponding wave functions (for the tetragonal case) are represented by shapes of the respective hole densities resolved according to S_z and L_z . Spin is indicated by color (red, up along z ; blue, down), orbital angular momentum by an arrow. The remaining $T_{x,y}$ are shown in the inset of (a). (c) Linear combinations of s and T_z forming the basis of the pseudospin $\tilde{S} = \frac{1}{2}$ model. For large negative Δ they converge to fully polarized states with antiparallel L and S . (d) Δ -dependent angles $\vartheta_{0,1}$ entering the wave functions. (e) xyz reference frame with z being the out-of-plane axis.

The auxiliary angle ϑ_0 is given by $\tan 2\vartheta_0 = 2\sqrt{2}/(1 - 2\delta)$ with $\delta = \Delta/\zeta$ and vanishes in $\Delta \rightarrow -\infty$ limit [see Fig. 1(d)]. The splitting of s and T_z levels equals $E_T = \frac{1}{4}\zeta[\sqrt{(1 - 2\delta)^2 + 8} - (1 - 2\delta)]$, vanishing as $\zeta/(1 - 2\delta)$.

The exchange interactions between d^4 ions in the above regime can be obtained by standard second-order perturbation theory in electron hopping resulting in a model for hardcore bosons s and T_z . These are subject to the local constraint $n_s + n_{T_z} = 1$, where $n_s = s^\dagger s$ and $n_{T_z} = T_z^\dagger T_z$ count bosons on a given site. The model becomes particularly transparent if formulated in terms of a pseudospin $\tilde{S} = \frac{1}{2}$ based on the linear combinations $|\tilde{\uparrow}\rangle, |\tilde{\downarrow}\rangle = \frac{1}{\sqrt{2}}(|s\rangle \pm i|T_z\rangle)$,

$$\begin{aligned} |\tilde{\uparrow}\rangle &= c^2|-1, +1\rangle - s^2|+1, -1\rangle - \sqrt{2}cs|0, 0\rangle, \\ |\tilde{\downarrow}\rangle &= c^2|+1, -1\rangle - s^2|-1, +1\rangle - \sqrt{2}cs|0, 0\rangle, \end{aligned} \quad (2)$$

with $c = \cos \frac{\vartheta_0}{2}$ and $s = \sin \frac{\vartheta_0}{2}$. This choice is motivated by the $\Delta \rightarrow -\infty$ limit depicted in Fig. 1(c) where $|\tilde{\uparrow}\rangle, |\tilde{\downarrow}\rangle$ correspond to fully polarized states $|-1, +1\rangle, |+1, -1\rangle$ with strictly antiparallel out-of-plane $L_z = -S_z$. Moreover, the pseudospin carries Van Vleck-type magnetic moment, which is purely out-of-plane with large $g_z = 6 \cos \vartheta_0$ and zero g_{xy} (see the SM [26]). On the operator level, this change of the basis is expressed via the correspondence relations $\tilde{S}_x = \frac{1}{2} - n_{T_z}$, $\tilde{S}_y = \frac{1}{2}(s^\dagger T_z + T_z^\dagger s)$, $\tilde{S}_z = -\frac{1}{2}(s^\dagger T_z - T_z^\dagger s)$. As a consequence, the level splitting E_T translates to a transverse field $h = E_T$ in the pseudospin formulation. The form of the exchange interactions can be easily anticipated by considering the $\Delta \rightarrow -\infty$ limit in Fig. 1(c). Since the two virtual electronic hoppings generating second-order exchange can only change the ionic spin component S_z by $\Delta S_z = 0, \pm 1$, the states $|\tilde{\uparrow}\rangle, |\tilde{\downarrow}\rangle$ with $S_z = \pm 1/2$ cannot be connected and the exchange is strictly of Ising $\tilde{S}_z \tilde{S}_z$ type in this limit. A full derivation for general $\Delta \lesssim -\zeta$ gives the pseudospin model

$$\mathcal{H}_{\tilde{S}} = \sum_{\langle ij \rangle} (J_z \tilde{S}_i^z \tilde{S}_j^z + J_x \tilde{S}_i^x \tilde{S}_j^x + J_y \tilde{S}_i^y \tilde{S}_j^y) - (h + \delta h) \sum_i \tilde{S}_i^x \quad (3)$$

with dominant J_z and $h = E_T$, supplemented by minor $J_x, J_y, \delta h$. In contrast to J_z , the latter exchange parameters only arise due to the small common parts of $|\tilde{\uparrow}\rangle, |\tilde{\downarrow}\rangle$ and as such they are proportional to $\sin^2 \vartheta_0$. As demonstrated later, they quickly drop when entering the $\Delta \lesssim -\zeta$ regime. Detailed exchange expressions for both 180° bonds (corner-sharing metal- O_6 octahedra) and 90° bonds (edge-sharing) as well as the connection to the hardcore boson formulations are given within the SM [26]. Note that due to the omission of the bond-directional states $T_{x,y}$, the interactions are identical for all bond directions. Neglecting the minor contributions in Eq. (3), we arrive at the final minimal model, which takes the form of transverse-field Ising model

$$\mathcal{H}_{\text{TFIM}} = J_z \sum_{\langle ij \rangle} \tilde{S}_i^z \tilde{S}_j^z - h \sum_i \tilde{S}_i^x. \quad (4)$$

Let us emphasize that this minimal model is imposed solely by the internal structure of the ionic states at sufficiently negative Δ/ζ , hence the mechanism is universal for any lattice.

Exchange parameters, phase diagrams, and excitations.

In this section, we illustrate the emergence of TFIM as a low-energy magnetic model by exploring phases and excitations obtained using an exchange model including all four low-energy states $s, T_{x,y,z}$ in the local basis. This model, to be

called (full) s - T model in the following, has the advantage to be applicable at any Δ/ζ and allows us to study the crossover to the $\Delta \lesssim -\zeta$ regime of interest. As we show below, the main features in this regime can indeed be understood and reproduced by simple AF TFIM. Its connection to the full s - T model is provided by projection onto s and T_z , which transforms the s - T model into the pseudospin- $\frac{1}{2}$ model of Eq. (3). On the way, we will also give quantitative hints on the TFIM parameters targeting Ru^{4+} compounds by the particular choice of Hubbard repulsion U , Hund's coupling J_H , and SOC strength ζ . The s - T model Hamiltonian was obtained by second-order perturbation theory and encompasses a large number of bond terms involving hardcore bosons s , $T_{x,y,z}$, following the general structure presented within the SM [26]. Due to this complexity, it cannot be given explicitly here (see [25] for a simpler version with $\Delta/\zeta = J_H/U = 0$), but we use it in full to determine the variational phase diagram using the trial product state

$$|\Psi_{\text{trial}}\rangle = \prod_{i \in \text{sites}} \left(\sqrt{1 - \rho_i} s^\dagger + \sqrt{\rho_i} \sum_{\alpha=x,y,z} d_{i\alpha}^* T_{i\alpha}^\dagger \right) |\text{vac}\rangle \quad (5)$$

and to calculate corresponding harmonic excitations using linear flavor wave theory (LFWT) [26,31–35]. $|\Psi_{\text{trial}}\rangle$ of Eq. (5) enables to capture various forms of magnetically ordered states linked to a condensation of hardcore vector bosons \mathbf{T} as well as the paramagnetic state where \mathbf{T} remain uncondensed. In the former case, the site-dependent variational parameters ρ_i (scalars) and \mathbf{d}_i (unit vectors) determine the condensate density and magnetic structure, respectively. The associated excitation spectrum contains magnon-like modes (fluctuations in \mathbf{d}) and amplitude mode (oscillations of the condensate density ρ). In the latter paramagnetic case, we find a trivial minimum with all $\rho_i = 0$ and excitations being carried directly by bosons \mathbf{T} .

As a first example, Fig. 2 gives an overview for a square lattice with straight 180° bonds, where the nearest-neighbor hopping t connects diagonally a pair of t_{2g} orbitals active on a given bond [24]. The phase diagram shown in Fig. 2(a) contains a window of paramagnetic (PM) phase around $\Delta/\zeta = 0$, separated by quantum critical points (QCP) at $\Delta \approx \pm\zeta$ from two condensed phases. Both are characterized by AF ordered Van Vleck moments but their nature strongly differs. The positive- Δ case with in-plane moments can be described by a pseudospin-1 model with predominantly XY-type of interactions and has been discussed in the context of Ca_2RuO_4 [26,29,30], which was estimated to have $\Delta/\zeta \approx 1.5$ [29]. In contrast, our negative- Δ case of interest is captured by the above pseudospin- $\frac{1}{2}$ TFIM. In this language, the pseudospins in the PM phase are fully aligned by the in-plane transverse field $h = E_T$, while beyond QCP they develop staggered out-of-plane component supported by $J_z > 0$. Due to zero in-plane g factor, only the AF out-of-plane component carries magnetic moment.

The TFIM picture is confirmed by the excitation spectra in Fig. 2(b). Near the QCP, the dispersion of the low-energy excitations probed by χ_{zz} susceptibility softens at the AF momentum $M = (\pi, \pi)$, deeper in the AF phase they become flat and the gap saturates, which is consistent with the expected Ising-type excitation at constant $\omega = 2J_z$ contrasting

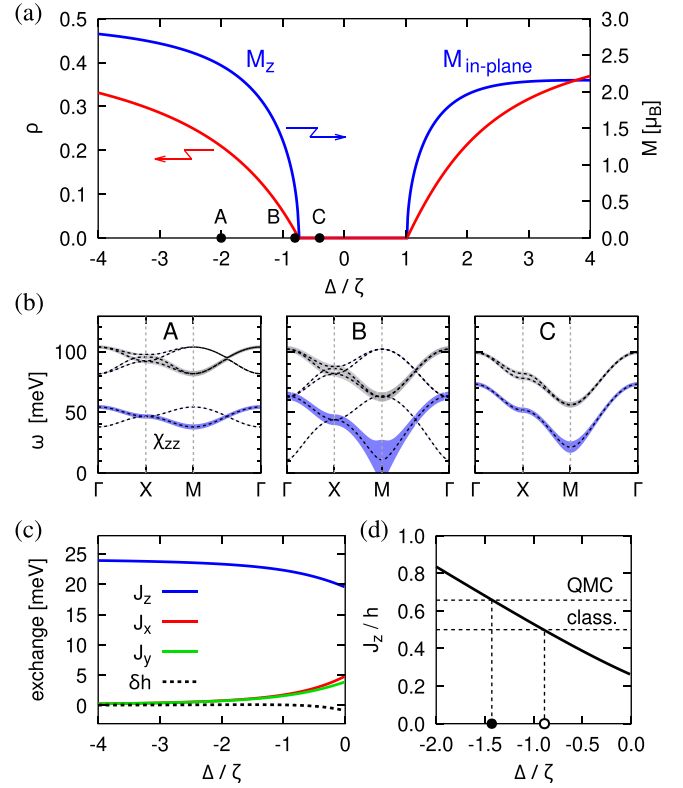


FIG. 2. (a) Variational phase diagram of the full s - T model for the square lattice obtained using $U = 3$ eV, $J_H = 0.5$ eV, $\zeta = 0.15$ eV (roughly corresponding to Ru^{4+}), and hopping $t = 0.14$ eV. At large enough negative/positive Δ , condensate of \mathbf{T} bosons with the density ρ is present and carries out-of-plane/in-plane AF moment. (b) Dynamic magnetic susceptibility calculated by LFWT at selected points in (a) and separated into zz component (blue) and in-plane $xx + yy$ part (gray). Line thickness scales with the intensity, dashed lines indicate the dispersions of excitations. Triangular Brillouin-zone path including high-symmetry points $\Gamma = (0, 0)$, $X = (\pi, 0)$, and $M = (\pi, \pi)$ is used. Identical zz component spectra are obtained also by LFWT limited to s and T_z bosons only. (c) Plot of the interaction parameters of the effective pseudospin- $\frac{1}{2}$ model (3) showing the clear dominance of J_z . (d) Parameter ratio J_z/h of the effective model plotted as function of Δ/ζ . The QCP position on Δ/ζ axis is estimated by mapping the critical ratio $(J_z/h)_{\text{crit}}$ of TFIM determined either classically (0.5) or using precise QMC result (≈ 0.657) back to Δ/ζ .

to the magnon-like excitations for positive Δ (see the SM [26]). The proximity to TFIM is illustrated by the evaluated parameters of the pseudospin- $\frac{1}{2}$ model (3) presented in Fig. 2(c). For $\Delta \lesssim -\zeta$, the dominant AF J_z quickly saturates at the infinite- Δ value $J_z \approx (5 - 7\eta)t^2/U$ with $\eta = J_H/U$ (see the SM [26]), and is accompanied by tiny in-plane $J_{x,y}$. Finally, Fig. 2(d) combines J_z of Fig. 2(c) and $h = E_T$ found in Fig. 1(a) into the ratio J_z/h that is the decisive parameter of TFIM and can be used to estimate the critical value of Δ/ζ . The value $(\Delta/\zeta)_{\text{crit}} \approx -0.9$ based on $(J_z/h)_{\text{crit}} = 0.5$ obtained by treating TFIM classically roughly agrees with our variational result for the full s - T model in Fig. 2(a). It gets corrected towards more negative $(\Delta/\zeta)_{\text{crit}} \approx -1.4$ when

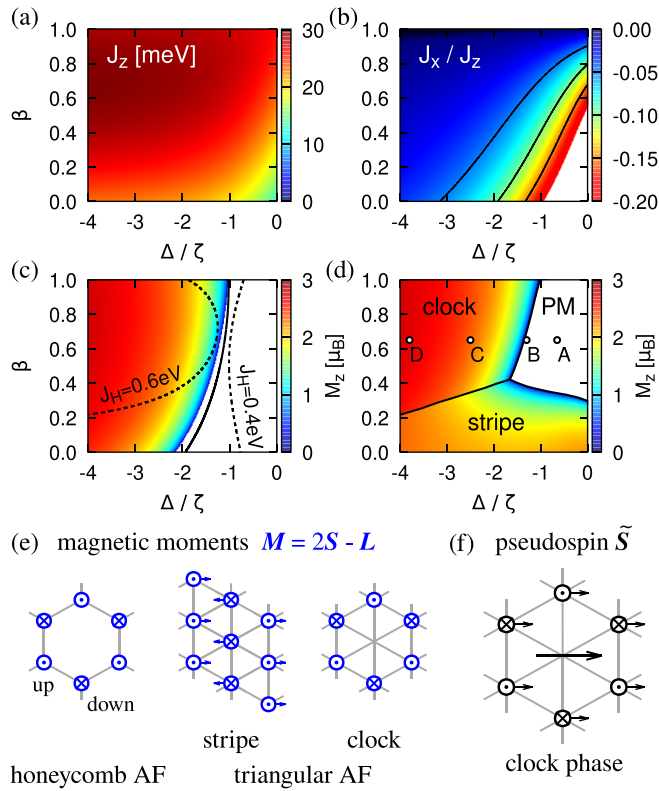


FIG. 3. (a) Effective exchange parameter J_z for the 90° bonding geometry and $U = 3$ eV, $J_H = 0.5$ eV, $\zeta = 0.15$ eV. The parameter β interpolates linearly between metal-O-metal hopping t and direct hopping t' , namely $t = (1 - \beta) \times 0.3$ eV, $t' = \beta \times 0.3$ eV. (b) Relative strength of J_x ($\approx J_y$) compared to the dominant J_z . (c) Variational phase diagram of the full s - T model on the honeycomb lattice. Major part is taken by AF phase with out-of-plane moments, the white area corresponds to the PM phase. The (classical) phase boundary of the resulting TFIM (i.e., pseudospin- $\frac{1}{2}$ model with $J_{x,y}$ neglected) is shown by the solid line. Dashed lines illustrate its trend for varying J_H . (d) Variational phase diagram for the triangular lattice. Using the critical ratios for TFIM from QMC [36] together with our TFIM parameters, the estimated phase boundary gets shifted horizontally by about 0.3 to the left in (c) and by 1.2 in (d). (e) Magnetic patterns of the phases in (c) and (d). (f) Clock-phase pattern in the pseudospin- $\frac{1}{2}$ representation. The central site carries a saturated in-plane moment, which is completely hidden in the magnetic pattern due to the zero in-plane g factor.

using the precise value $(J_z/h)_{\text{crit}} \approx 0.657$ obtained by QMC [37].

Similar analysis is performed for 90° bond geometry that occurs in, e.g., honeycomb or triangular lattices with edge-sharing octahedra. Here two major hopping channels active on metal₂-O₂ plaquettes have to be simultaneously considered—bonding paths via oxygen ions and a direct overlap of d orbitals [24]. The former hopping with amplitude t connects off-diagonally a bond-dependent pair of t_{2g} orbitals while the complementary t_{2g} orbital is subject to direct hopping t' . Despite the completely different hopping rules as compared to the 180° case, the pseudospin- $\frac{1}{2}$ interactions plotted in Figs. 3(a) and 3(b) again feature dominant AF Ising J_z accompanied by minor in-plane $J_{x,y}$, in accord with the general

conclusions of the previous section. For large negative Δ , the value of J_z approaches $J_z \approx \frac{4}{9} [(7 - 20\eta)t^2 + (2 + 8\eta)tt' + (4 - 8\eta)t'^2]/U$.

Variational phase diagram for the nonfrustrated honeycomb lattice presented in Fig. 3(c) and the corresponding excitation spectrum (see the SM [26]) show similar behavior as for the square lattice. Much richer is the case of the frustrated triangular lattice. The phase diagram shown in Fig. 3(d) contains two condensed phases with nontrivial patterns depicted in Figs. 3(e) and 3(f). One of them appears in so-called clock phase familiar from the studies of TFIM on triangular lattice [13,14]. Here the frustration of pseudospins is resolved by a formation of honeycomb AF pattern of the out-of-plane components to satisfy the Ising interactions and a simultaneous alignment of the in-plane components with the transverse field. At the remaining sites, the pseudospins are strictly in-plane, avoiding the Ising interactions and conforming fully to the transverse field. The other pattern—of stripy type—is specific to our s - T model and is not captured by the pseudospin- $\frac{1}{2}$ TFIM because of the participation of $T_{x,y}$ in the condensate. Based on the extended nature of $4d$ and $5d$ orbitals, the regime $t' \gtrsim t$ can be expected, making the clock phase more relevant.

Interestingly, the clock pattern of pseudospins on triangular lattice is obscured by zero in-plane g factor, giving rise to a static magnetic pattern identical to that of the honeycomb AF phase. However, the excitation spectra reveal a fundamental difference to the latter case. Figure 4(a) shows the evolution of the magnetic excitations when crossing the PM/clock boundary. These are again obtained using the full s - T model, but—as demonstrated by Fig. 4(b)—the relevant χ_{zz} is perfectly reproduced also by the pseudospin dynamics within the corresponding TFIM. Approaching the PM/clock boundary, the excitations soften at the characteristic momentum $K = 2\pi(\frac{1}{\sqrt{3}}, \frac{1}{3})$ of the honeycomb AF pattern formed after entering the clock phase. Here a separation of energy scales occurs. The high-energy part of the spectrum is represented by a flat Ising-type excitation at $\omega \approx 2J_z$ encountered previously and linked here to a pseudospin flip taking place in the honeycomb AF structure. This excitation is complemented by a dispersing low-energy mode (energy scale h) that involves rotations of in-plane pseudospins. Its dispersion, soft near K , is approximately given by $\omega_q \approx h[1 - (h/h_c)|\gamma_q|^2]$ with $\gamma_q = 2 \cos(\frac{\sqrt{3}}{2}q_x) + \exp(i\frac{3}{2}q_y)$ and $h_c = \frac{3}{2}J_z$ denoting the critical transverse field. Remarkably, this intense magnetic excitation stems from the moments that are magnetically invisible in the static pattern. In contrast to the triangular lattice case, the honeycomb spectrum (see the SM [26]) hosts only the Ising-type excitation and its low-energy part is empty.

Conclusions. We presented a detailed theoretical account on the exchange interactions in $4d^4$ and $5d^4$ spin-orbit Mott insulators in the regime of negative tetragonal or trigonal crystal field Δ . As illustrated by the corresponding phase diagrams and excitations for several 2D lattices, the low-energy magnetism can be well captured by AF transverse-field Ising model involving effective spins- $\frac{1}{2}$. Being based on d valence electrons, the emergent TFIM features convenient energy scales in the range of tens of meV. The transverse field is intrinsic, generated by CF itself, and is therefore sensitive to strain control. Robust Ising-type interactions are imposed

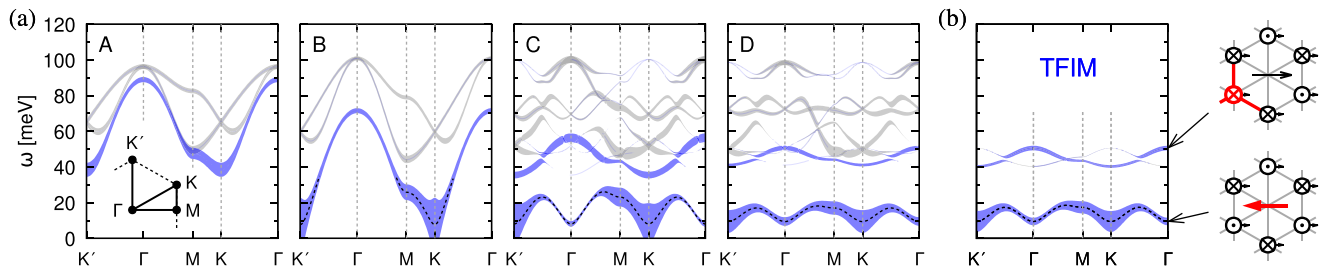


FIG. 4. (a) Magnetic excitation spectra for the selected points indicated in Fig. 3(d) as obtained by LFWT applied to s - T model. The intensity is represented by line thickness as in Fig. 2(b) with blue indicating the out-of-plane zz component and gray the in-plane components. The inset shows the Brillouin zone path. (b) zz susceptibility for the point D calculated using linear spin-wave theory applied to the corresponding TFIM with $J_z \approx 30$ meV and $h \approx 19$ meV. Cartoons capture the two distinct excitations—low-energy fluctuations of the in-plane pseudospins and high-energy Ising-type excitations.

by the internal spin-orbital structure of the d^4 ionic states, and as such they are generic to both 180° and 90° bonding geometries. This universality of TFIM description is in strong contrast to the much different behavior of singlet-triplet models obtained for $\Delta/\zeta = 0$ in these two bonding-geometry cases [25,27,28]. The radical change of the magnetic model when varying Δ/ζ is an excellent illustration of the richness of the exchange interactions among $4d$ and $5d$ ions brought about by the complex structure of the low-energy ionic states. Apart from promising an identification/engineering of TFIM

in the family of $4d$ and $5d$ correlated oxides, the proposed scenario also motivates the study of related theoretical issues. For example, the calculations suggest the dominant Ising exchange to be accompanied by small interactions between transverse components of effective spins. Their influence on the BKT behavior of TFIM is an interesting open problem.

Acknowledgments. Stimulating discussions with Giniyat Khaliullin are gratefully acknowledged. This work was supported by Czech Science Foundation (GAČR) under Project No. GA22-28797S.

- [1] P. G. de Gennes, Collective motions of hydrogen bonds, *Solid State Commun.* **1**, 132 (1963).
- [2] S. Sachdev, *Quantum Phase Transitions* (Cambridge University Press, Cambridge, 2011).
- [3] A. Dutta, G. Aeppli, B. K. Chakrabarti, U. Divakaran, T. F. Rosenbaum, and D. Sen, *Quantum Phase Transitions in Transverse Field Spin Models: From Statistical Physics to Quantum Information* (Cambridge University Press, Cambridge, 2015).
- [4] E. Ising, Beitrag zur Theorie des Ferromagnetismus, *Z. Phys.* **31**, 253 (1925).
- [5] L. Onsager, Crystal statistics. I. A two-dimensional model with an order-disorder transition, *Phys. Rev.* **65**, 117 (1944).
- [6] B. Kaufman, Crystal statistics. II. Partition function evaluated by spinor analysis, *Phys. Rev.* **76**, 1232 (1949).
- [7] B. Kaufman and L. Onsager, Crystal statistics. III. Short-range order in a binary Ising lattice, *Phys. Rev.* **76**, 1244 (1949).
- [8] G. H. Wannier, Antiferromagnetism. The triangular Ising net, *Phys. Rev.* **79**, 357 (1950).
- [9] G. H. Wannier, Antiferromagnetism. The triangular Ising net, *Phys. Rev. B* **7**, 5017(E) (1973).
- [10] C. Castellano, S. Fortunato, and V. Loreto, Statistical physics of social dynamics, *Rev. Mod. Phys.* **81**, 591 (2009).
- [11] D. Sornette, Physics and financial economics (1776–2014): puzzles, Ising and agent-based models, *Rep. Prog. Phys.* **77**, 062001 (2014).
- [12] R. Moessner, S. L. Sondhi, and P. Chandra, Two-dimensional periodic frustrated Ising models in a transverse field, *Phys. Rev. Lett.* **84**, 4457 (2000).
- [13] R. Moessner and S. L. Sondhi, Ising models of quantum frustration, *Phys. Rev. B* **63**, 224401 (2001).
- [14] S. V. Isakov and R. Moessner, Interplay of quantum and thermal fluctuations in a frustrated magnet, *Phys. Rev. B* **68**, 104409 (2003).
- [15] R. B. Stinchcombe, Ising model in a transverse field. I. Basic theory, *J. Phys. C: Solid State Phys.* **6**, 2459 (1973).
- [16] R. Coldea, D. A. Tennant, E. M. Wheeler, E. Wawrzynska, D. Prabhakaran, M. Telling, K. Habicht, P. Smeibidl, and K. Kiefer, Quantum criticality in an Ising chain: Experimental evidence for emergent E_8 symmetry, *Science* **327**, 177 (2010).
- [17] H. Li, Y. D. Liao, B.-B. Chen, X.-T. Zeng, X.-L. Sheng, Y. Qi, Z. Y. Meng, and W. Li, Kosterlitz-Thouless melting of magnetic order in the triangular quantum Ising material TmMgGaO_4 , *Nat. Commun.* **11**, 1111 (2020).
- [18] Z. Hu, Z. Ma, Y.-D. Liao, H. Li, C. Ma, Y. Cui, Y. Shangguan, Z. Huang, Y. Qi, W. Li *et al.*, Evidence of the Berezinskii-Kosterlitz-Thouless phase in a frustrated magnet, *Nat. Commun.* **11**, 5631 (2020).
- [19] Z. Dun, M. Daum, R. Baral, H. E. Fischer, H. Cao, Y. Liu, M. B. Stone, J. A. Rodriguez-Rivera, E. S. Choi, Q. Huang, H. Zhou, M. Mourigal, and B. A. Frandsen, Neutron scattering investigation of proposed Kosterlitz-Thouless transitions in the triangular-lattice Ising antiferromagnet TmMgGaO_4 , *Phys. Rev. B* **103**, 064424 (2021).
- [20] Y. Shen, C. Liu, Y. Qin, S. Shen, Y.-D. Li, R. Bewley, A. Schneidewind, G. Chen, and J. Zhao, Intertwined dipolar and multipolar order in the triangular-lattice magnet TmMgGaO_4 , *Nat. Commun.* **10**, 4530 (2019).

- [21] C. Liu, F.-Y. Li, and G. Chen, Upper branch magnetism in quantum magnets: Collapses of excited levels and emergent selection rules, *Phys. Rev. B* **99**, 224407 (2019).
- [22] G. Chen, Intrinsic transverse field in frustrated quantum Ising magnets: Physical origin and quantum effects, *Phys. Rev. Res.* **1**, 033141 (2019).
- [23] C. Liu, C.-J. Huang, and G. Chen, Intrinsic quantum Ising model on a triangular lattice magnet TmMgGaO_4 , *Phys. Rev. Res.* **2**, 043013 (2020).
- [24] T. Takayama, J. Chaloupka, A. Smerald, G. Khaliullin, and H. Takagi, Spin-orbit-entangled electronic phases in $4d$ and $5d$ transition-metal compounds, *J. Phys. Soc. Jpn.* **90**, 062001 (2021).
- [25] G. Khaliullin, Excitonic magnetism in Van Vleck-type d^4 Mott insulators, *Phys. Rev. Lett.* **111**, 197201 (2013).
- [26] See Supplemental Material at <http://link.aps.org/supplemental/10.1103/PhysRevB.109.L020403> for additional technical details and susceptibility spectra. It includes Refs. [24,25,28,29,31–35].
- [27] P. S. Anisimov, F. Aust, G. Khaliullin, and M. Daghofer, Nontrivial triplon topology and triplon liquid in Kitaev-Heisenberg-type excitonic magnets, *Phys. Rev. Lett.* **122**, 177201 (2019).
- [28] J. Chaloupka and G. Khaliullin, Highly frustrated magnetism in relativistic d^4 Mott insulators: Bosonic analog of the Kitaev honeycomb model, *Phys. Rev. B* **100**, 224413 (2019).
- [29] A. Jain, M. Krautloher, J. Porras, G. H. Ryu, D. P. Chen, D. L. Abernathy, J. T. Park, A. Ivanov, J. Chaloupka, G. Khaliullin, B. Keimer, and B. J. Kim, Higgs mode and its decay in a two-dimensional antiferromagnet, *Nat. Phys.* **13**, 633 (2017).
- [30] S.-M. Souliou, J. Chaloupka, G. Khaliullin, G. Ryu, A. Jain, B. J. Kim, M. Le Tacon, and B. Keimer, Raman scattering from Higgs mode oscillations in the two-dimensional antiferromagnet Ca_2RuO_4 , *Phys. Rev. Lett.* **119**, 067201 (2017).
- [31] N. Papanicolaou, Pseudospin approach for planar ferromagnets, *Nucl. Phys. B* **240**, 281 (1984).
- [32] N. Papanicolaou, Unusual phases in quantum spin-1 systems, *Nucl. Phys. B* **305**, 367 (1988).
- [33] A. V. Chubukov, Fluctuations in spin nematics, *J. Phys.: Condens. Matter* **2**, 1593 (1990).
- [34] A. Joshi, M. Ma, F. Mila, D. N. Shi, and F. C. Zhang, Elementary excitations in magnetically ordered systems with orbital degeneracy, *Phys. Rev. B* **60**, 6584 (1999).
- [35] T. Sommer, M. Vojta, and K. W. Becker, Magnetic properties and spin waves of bilayer magnets in a uniform field, *Eur. Phys. J. B* **23**, 329 (2001).
- [36] Y.-C. Wang, Y. Qi, S. Chen, and Z. Y. Meng, Caution on emergent continuous symmetry: A Monte Carlo investigation of the transverse-field frustrated Ising model on the triangular and honeycomb lattices, *Phys. Rev. B* **96**, 115160 (2017).
- [37] C.-J. Huang, L. Liu, Y. Jiang, and Y. Deng, Worm-algorithm-type simulation of the quantum transverse-field Ising model, *Phys. Rev. B* **102**, 094101 (2020).